# Highly stretchable, sensitive and wide linear responsive fabric-based strain sensors with a self-segregated carbon nanotube (CNT)/Polydimethylsiloxane (PDMS) coating

Progress in Natural Science: Materials International 32 (2022) 34–42

HOSTED BY

Contents lists available at ScienceDirect

Progress in Natural Science: Materials International

journal homepage: www.elsevier.com/locate/pnsmi

# Highly stretchable, sensitive and wide linear responsive fabric-based strain sensors with a self-segregated carbon nanotube (CNT)/ Polydimethylsiloxane (PDMS) coating

Libing Liu [a,1], Xuezhong Zhang [a,1], Dong Xiang [a,*], Yuanpeng Wu [a,e], Dan Sun [b], Jiabin Shen [c], Menghan Wang [d], Chunxia Zhao [a], Hui Li [a], Zhenyu Li [a], Ping Wang [a], Yuntao Li [a,**]

[a] School of New Energy and Materials, Southwest Petroleum University, Chengdu, 610500, China
[b] School of Mechanical and Aerospace Engineering, Queen's University Belfast, Belfast, BT9 5AH, UK
[c] State Key Laboratory of Polymer Materials Engineering, Polymer Research Institute of Sichuan University, Chengdu, 610065, China
[d] College of Materials Science and Engineering, Chongqing University, Chongqing, 400030, China
[e] The Center of Functional Materials for Working Fluids of Oil and Gas Field, Southwest Petroleum University, Chengdu, 610500, China

ARTICLE INFO

*Keywords:*
Strain sensor
Self-segregated structure
Carbon nanotubes
Polydimethylsiloxane
Nanocomposites

ABSTRACT

Flexible strain sensors have received increasing attention with the development of wearable electronic devices. However, integrating wide strain detection range, high sensitivity while maintaining relatively wide linear response range for such sensor system still remain a challenge. A fabric based flexible sensor (S-CNT/PDMS-F) was designed and fabricated, and the sensor can simultaneously achieve high sensitivity, wide linear response and strain detection range by combining self-segregated carbon nanotube (CNT)/polydimethylsiloxane (PDMS) composites and elastic medical bandage. It has been observed that this new sensor system can achieve a high sensitivity with a gauge factor of 615, a large linear responsive range of 0–100% strain ($R^2 = 0.993$) and a wide strain detection range of ~ 200%, which is superior to almost all the reported CNT/PDMS flexible strain sensors. Compared to the similar fabric based strain sensor system deploying non self-segregated structure (C-CNT/PDMS-F), our S-CNT/PDMS-F demonstrates higher electrical conductivity and lower electrical percolation threshold and response time of 55 ms, as well as more stable and repeatable performance under cyclic loading conditions. The capability of the sensors in monitoring physiological activities and weight distribution has also been demonstrated.

## 1. Introduction

With the rapid development of flexible electronic devices, the demand for high performance conductive polymer composites (CPCs) has steadily increased in many fields, such as medical equipment, human-machine interactions, and soft robotics [1–3]. In recent years, CPCs consisting of conductive nanofillers embedded within an insulating elastic polymer matrix have been widely used in wearable electronic devices such as flexible strain sensors due to their simple and low-cost preparation processes, controllable electrical conductivity, and excellent mechanical and electrical properties [4–7]. To date, flexible strain sensors are considered the core technology for wearable electronic devices [8,9] and have received increasing attention from both academia and industry. Flexible strain sensors with a wide strain detection range, high sensitivity, excellent stability, repeatability and durability are of particular interest to meet the imperative demands of various high-end applications, such as human motion monitoring, electronic skins, and "smart" prosthetics [10–13].

Due to their excellent mechanical properties and high electrical conductivity, carbon nanomaterials such as CNTs, have been widely explored in sensing applications [14]. Strain detection range and sensitivity are considered as the key performance indices for CPC-based strain sensors. The sensitivity of the sensors is described by gauge factor (GF):

* Corresponding author.
** Corresponding author.
*E-mail addresses:* dxiang01@hotmail.com (D. Xiang), yuntaoli@swpu.edu.cn (Y. Li).
[1] These authors contributed equally to this work.

https://doi.org/10.1016/j.pnsc.2021.10.012
Received 7 July 2021; Received in revised form 17 October 2021; Accepted 24 October 2021
Available online 19 November 2021

**Table 1**
A summary of the performance and preparation methods of CNT/PDMS based strain sensors.

| Material[a] | Stretchability | Maximum GF | Linear response range | Percolation threshold | Conductive network structure | Main process | Reference |
|---|---|---|---|---|---|---|---|
| CNT/PDMS | 0–30% | 4.36 | 0–10% | 0.13 vol% (0.24 wt%) | random | Mixed solution | [15] |
| CB/CNT/PDMS | 0–300% | 13.1 | 0–50% | / | random | Mixed solution | [23] |
| CNT/SF/PDMS | 0–1.4% | 23 | 0–1% | / | random | Mixed solution | [24] |
| self-segregated CNT/PDMS | 0–30% | 42.5 | 0–15% | 0.003 vol% (0.0055 wt%) | segregated | Mixed solution Introducing segregated phase | [21] |
| $SiO_2$/CNT/PDMS | 0–41% | 62.9 | 0–8% | / | random | Mixed solution | [25] |
| S-CNT/PDMS-F | 0–200% | 615 | 0–100% | 0.51 wt% | segregated | Mixed solution Introducing segregated phase coating | This work |

[a] SF: silicone fluid; S-CNT/PDMS-F: the self-segregated CNT/PDMS fabric-based sensor.

$$GF = \frac{\Delta R}{R_0 \varepsilon} \quad (1)$$

where ε, ΔR and $R_0$ represent the applied strain, resistance change under the applied strain, and initial resistance, respectively.

In recent years, many researchers have sought to combine CNT with highly stretchable polymeric material such as PDMS to prepare CPCs based strain sensors with enhanced performance indices. For instance, Zheng et al. [15] prepared carbon black (CB)/PDMS and CNT/PDMS nanocomposite strain sensors with a strain detection range of 0–30% and GF of 15.75 and 4.36, respectively. Choi et al. [16] prepared star-shaped CNT/PDMS strain sensor that could identify the direction of the applied strain. The sensor had a strain detection range of 0–50%, but the maximum GF was only 0.11 (0–5%). Wearable strain sensors based on a thermoplastic polyurethane (TPU)/CNT/PDMS nanofiber composite were prepared by Wang et al. [17]. The sensors had a strain detection range of 0–100%, but the maximum GF was only 0.339 for applied strain 50–100%. Although conductive networks have been successfully established in these CPCs, the strain detection range and sensitivity of the above mentioned sensor systems are still yet to be optimized for high performance strain sensing applications.

To further enhance the performance of nanocarbon/PDMS based nanocomposite strain sensors, Ma et al. [18] fabricated a graphene (G)/PDMS/reduced graphene oxide (RGO) strain sensor with a self-compensated two-order conductive network. The G/PDMS/RGO strain sensor could achieve a wide strain detection range (0–350%) and ultrahigh sensitivity (maximum GF = 88443). A similar two-order conductive network structured Au/single-walled CNT/PDMS strain sensor was also developed by Sun et al., with wide strain detection range (100% strain) and high sensitivity (GF: $7.1 \times 10^4$ to $3.4 \times 10^6$) [1]. In order to establish the required conductive network structure (percolation network) in the above sensor designs, high concentration of nanofillers was required, which not only increases the processing difficulty and manufacturing cost, but also could lead to increased particle agglomeration and compromise the nanocomposites integrity/mechanical properties [19,20].

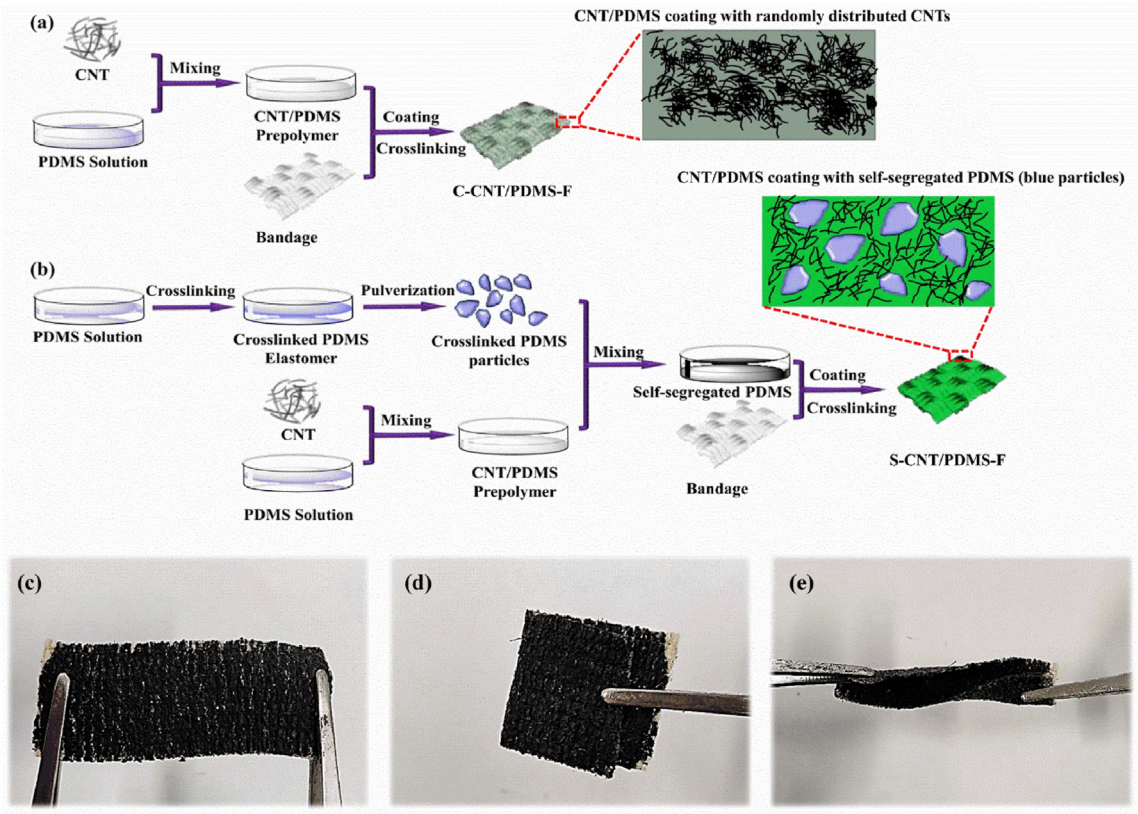


**Fig. 1.** Schematic diagram showing preparation process and conductive network of (a) C-CNT/PDMS-F and (b) S-CNT/PDMS-F. Photographs of a stretched (c), folded (d) and twisted (e) S-CNT/PDMS-F.

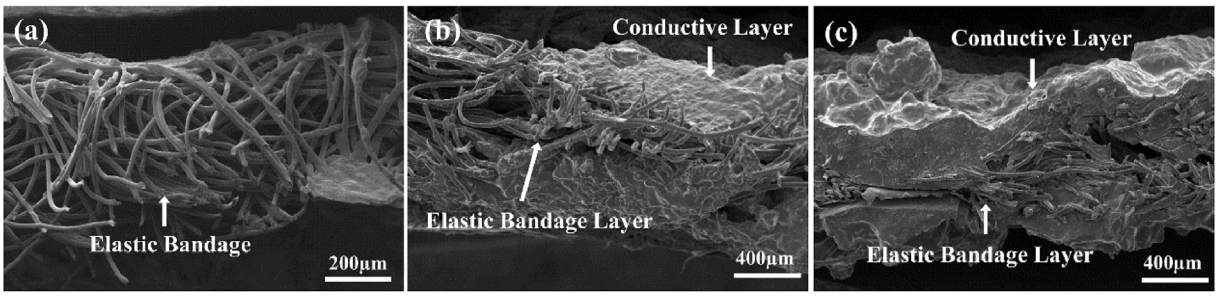


**Fig. 2.** SEM images of the elastic bandage (a), C-CNT/PDMS-F (b) and S-CNT/PDMS-F(c).

A strategy to alleviate the above mentioned drawback is to introduce segregated structures within CPCs to reduce the percolation threshold of conductive nanofillers. For example, Wang et al. [21] created self-segregated structure in CNT/PDMS nanocomposites, in which the cross-linked PDMS particles acted as the self-segregated phase. The ultralow percolation threshold (0.003 vol% CNTs) achieved was mainly ascribed to the confined distribution of the MWCNTs within the PDMS continuous phase and the three-dimensional (3D) conductive networks formed by the segregated structure. Although the reported strain sensor achieved an ultralow percolation threshold, the strain detection range (0–30%) and its sensitivity (GF = 42.5) remained relatively low. Moreover, the sensor only showed linear response within a very limited strain range (~15%), which present a challenge in the sensor calibration [22]. Table 1 lists the CNT/PDMS nanocomposite based strain sensors developed in recent years, with details of their preparation methods and performance indices. It can be seen that integrating wide strain detection range, high sensitivity while maintaining relatively wide linear response range for such sensor system still remain a challenge.

Here, a self-segregated CNT/PDMS nanocomposite with a good phase compatibility has been prepared and applied as a coating on elastic medical bandage to obtain a self-segregated CNT/PDMS fabric-based strain sensor. The resulting sensor system has a wide strain detection range, high sensitivity, linearity in response, and high repeatability. The strain sensor has been demonstrated for a range of wearable sensing devices including human motion detection, loading condition monitoring, and recognizing object weight distribution. These promising results demonstrate the strong potential of our low cost sensor system for wide ranging applications such as motion detection, health monitoring, human-machine interactions and intelligent robotics, etc.

## 2. Experimental

### 2.1. Materials

CNTs (NC7000) with diameter ~ 9.5 nm and average length ~ 1.5 μm were obtained from Nanocyl S.A (Belgium). The elastic medical bandage was purchased from Zhejiang Kanglidi Medical Supplies Co., Ltd (China). Polyvinylpyrrolidone (PVP, K-30) and dichloromethane (DCM) were obtained from the Chengdu Cologne Chemical Reagent Company, China. PDMS base and curing agent (DC184) were supplied by the Dow Corning Corporation, America.

### 2.2. Preparation of the conventional and self-segregated strain sensors

Conventional CNT/PDMS (i.e. without self-segregation) fabric-based samples with varying CNT mass fraction (0–3 wt%) were prepared following the procedure illustrated in Fig. 1a. The CNTs and PVP were dispersed in DCM by sonication at 100 W and 40 kHz for 1 h at 20 °C to obtain a homogeneous CNT suspension. PDMS base and the curing agent (weight ratio = 10: 1) were added to the CNT suspension and magnetically stirred for 2 h at room temperature. DCM was then removed to obtain the CNT/PDMS prepolymer. The CNT/PDMS prepolymer was coated onto the elastic medical bandages (50 × 25 × 0.5 $mm^3$) by a brush-coating process. The resulting bandages were cured in an oven for 2 h at 80 °C. The resulting CNT/PDMS fabric-based sensor was named as C-CNT/PDMS-F.

For the self-segregated CNT/PDMS fabric-based sensor (S-CNT/PDMS-F), the PDMS base and the curing agent (weight ratio = 10: 1) were mixed, degassed, and cured for 2 h at 80 °C to obtain 10 mm thick PDMS sheets. The cured PDMS sheets then were pulverized into 250–425 μm particles using a high-speed mechanical pulverizer (FW100, Tianjin Taisite Ltd, China) after frozen in liquid nitrogen for 10 min, as shown in Fig. 1b. CNTs and PDMS base were mixed at different ratios via ultrasonication in DCM at 100 W and 40 kHz for 1 h at 20 °C. DCM was then evaporated to obtain the uncrosslinked CNT/PDMS base. Afterwards, curing agent and cross-linked PDMS particles were added to the uncrosslinked CNT/PDMS prepolymer and mixed thoroughly. The weight ratio of prepolymer and cross-linked PDMS particles was 5: 1. Other weight ratios were also trialed, however higher crosslinked PDMS particle content led to a poor coating quality, whereas lower crosslinked PDMS particle content led to the vastly reduced effect of the self-segregated structure. The CNT/PDMS prepolymer was degassed and coated onto both sides of the elastic bandages by a brush-coating process, and the coated-bandages were cured at 80 °C for 2 h to obtain the CNT/PDMS nanocomposite coating with a self-segregated structure (Fig. 1b). Conductive copper wire electrodes were then attached to both ends of the sensor samples using conductive silver paste (Nanjing Xili Special Adhesive Co., Ltd, China).

Fig. 1c, d and e show that S-CNT/PDMS-F have excellent flexibility – they can be stretched, folded, and twisted, showing their potential for wearable electronic devices.

### 2.3. Characterization

The cross-section of samples was studied using a FEI Quanta 650 FEG field emission scanning electron microscope (FESEM) with platinum sputtering at an accelerating voltage of 10 kV. To further analyze the distributions of the CNTs within S-CNT/PDMS-F and C-CNT/PDMS-F, the samples were directly observed without platinum sputtering using the FESEM at an accelerating voltage of 20 kV. The conductive network based on the rich secondary electrons emitted from the conductive CNTs was observed.

The electrical conductivity (σ) of S-CNT/PDMS-F and C-CNT/PDMS-F were measured using the two-point method [7] with a DC digital source meter (Tektronix PWS4323) and picoamp-meter (Keithley 6485) at applied voltage of 3 V. The sensors had an electrode distance of 30 mm σ of the sensors was calculated according to:

$$\sigma = \frac{1}{R} \times \frac{L}{S} \tag{2}$$

where R is the electrical resistance of the sensor, L and S are the electrode distance and cross-sectional area of the sensor, respectively.

The electromechanical performance of S-CNT/PDMS-F and C-CNT/PDMS-F was measured using the universal tester (MTS CMT4104)

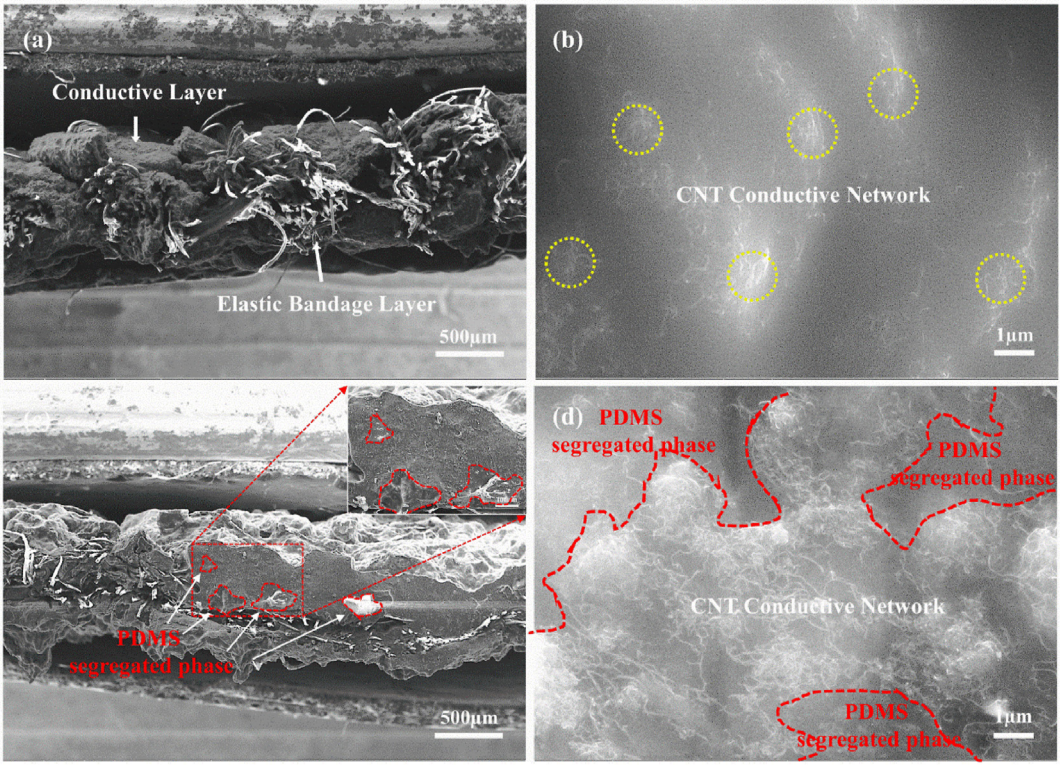


**Fig. 3.** Cross-sectional SEM images of (a), (b) C-CNT/PDMS-F and (c), (d) S-CNT/PDMS-F sensors with 3 wt% MWCNTs. Red contour highlights the segregated PDMS particles.

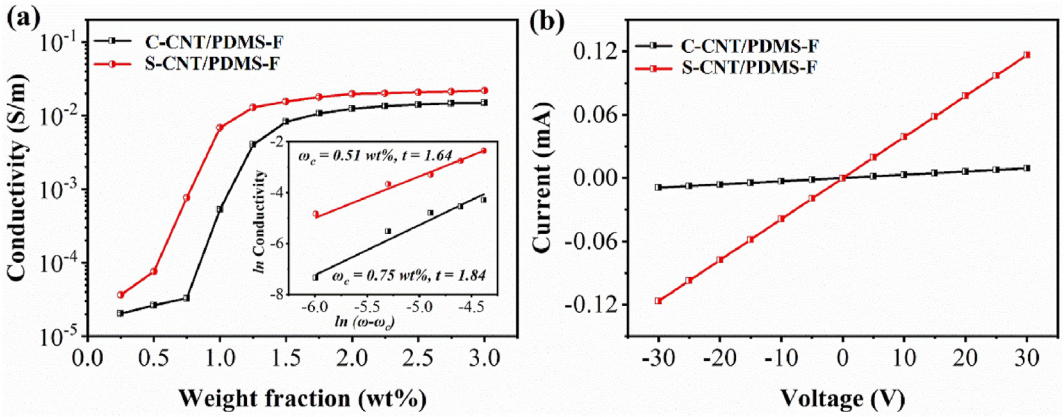


**Fig. 4.** (a) Volume conductivity of S-CNT/PDMS-F and C-CNT/PDMS-F with different CNTs wt%. (b) Current-voltage curves for S-CNT/PDMS-F and C-CNT/PDMS-F.

equipped with the DC digital source meter and picoamp-meter at applied voltage of 3 V.

## 3. Results and discussion

### 3.1. Morphological and structural analysis of the strain sensors

Fig. 2a shows that the surface of the as-purchased elastic medical bandage was composed of smooth fibers. Fig. 2b and c show that S-CNT/PDMS-F and C-CNT/PDMS-F had a sandwiched structure, with the bandage fabric in between the top and bottom conductive CNT/PDMS composite layers (~400 μm). From Fig. 3, it can be seen that CNTs were randomly distributed within the C-CNT/PDMS-F layers and partially aggregated CNTs (yellow dashed circle in Fig. 3b) during the preparation process resulted in a relatively weak conductive network. In contrast, the cross-linked PDMS particles in S-CNT/PDMS-F formed segregated "islands" (red dashed contours in Fig. 3c). Subsequently, the CNTs were mostly constrained within the channels formed between the cross-linked PDMS particles (Fig. 3d). As such, the CNTs formed a denser conductive network due to the excluded volume effect with the segregated PDMS phase that occupied part of the continuous CNT/PDMS phase [26].

### 3.2. Electrical properties of the strain sensors

Fig. 4 compares the electrical properties of S-CNT/PDMS-F and C-CNT/PDMS-F. As can be seen in Fig. 4a, the conductivity measured for both sensors showed similar trends, i.e., conductivity increased with increasing CNT wt%. A classic percolation behavior was also observed for S-CNT/PDMS-F and C-CNT/PDMS-F, respectively. However, at each given CNT wt%, the conductivity of S-CNT/PDMS-F was higher than that of C-CNT/PDMS-F. This difference signifies the much improved conductivity of the S-CNT/PDMS-F sensor. The higher conductivity was due

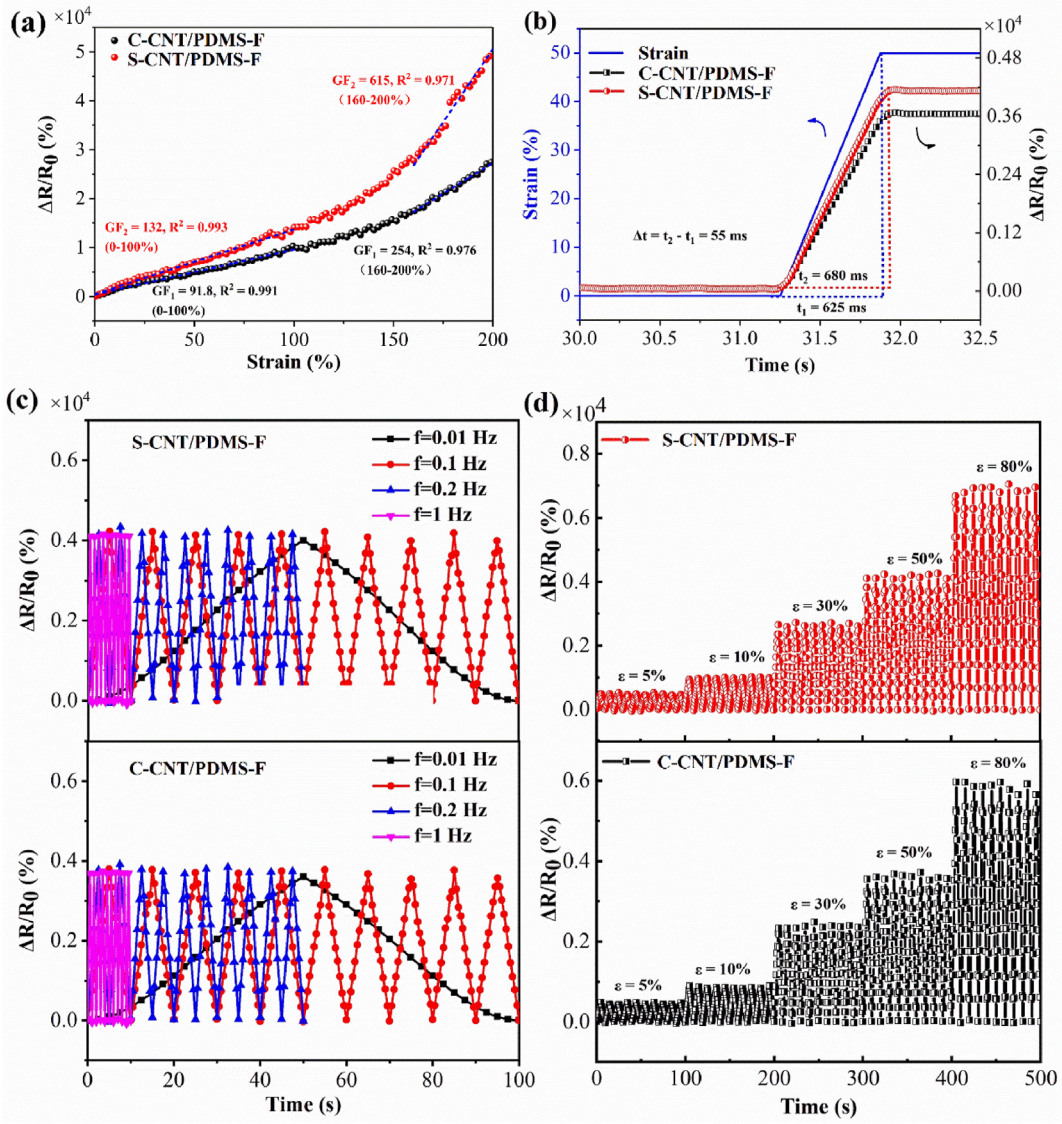


**Fig. 5.** Performance comparison between C-CNT/PDMS-F and S-CNT/PDMS-F (a) Relationship between $\Delta R/R_0$ and the applied strain. (b) The response time under cyclic loading/unloading processes. (c) Variation in $\Delta R/R_0$ during cyclic loading at 50% strain and at frequencies of 0.01, 0.1, 0.2, and 1 Hz. (d) $\Delta R/R_0$ under loading/unloading cycles under different strains (5%, 10% 30%, 50% and 80%) at 0.1Hz.

to the excluded volume effect of the cross-linked PDMS particles which made the CNTs distribution more compact along the conductive pathways (Fig. 3d). The better contacts between the CNTs lowers the resistance. The CNT percolation threshold can be determined following the classical percolation theory [27].

$$\sigma(\omega) = B(\omega - \omega_c)^t \tag{3}$$

where $\sigma(\omega)$ is the volume conductivity of the strain sensor, B is a scale factor, $\omega$ is CNT wt% in the CPCs, $\omega_c$ is the percolation threshold of the strain sensor, and t is a parameter that depends on the dimension of the conductive network. t is in the range of 1–1.3 for 2D conductive networks and in the range of 1.6–2 for 3D conductive networks [28].

Fig. 4a shows the curve fitting for determining $\omega_c$ and t of the two sensors under testing. The t values for S-CNT/PDMS-F and C-CNT/PDMS-F were 1.64 and 1.84, respectively, suggesting establishment of 3D conductive networks in both sensors. Further, $\omega_c$ was 0.51 wt% and 0.75 wt% for S-CNT/PDMS-F and C-CNT/PDMS-F, respectively. As expected, the percolation threshold of S-CNT/PDMS-F was 1.47 times lower than that of C-CNT/PDMS-F. The percolation threshold of S-CNT/PDMS-F was also much lower than what was previously reported other non-aggregated CNT/PDMS based sensors [29] and many other CPCs [27, 30]. The cross-linked PDMS particles within S-CNT/PDMS-F occupied a large volume of the nanocomposite, which meant that the CNTs were more concentrated in the non-segregated PDMS phase, and thus a lower CNT wt% was required to form a percolated network. However, the percolation threshold is higher than that presented in Ref. [21], which could be attributed to lower cross-linked PDMS content used.

Fig. 4b shows that the measured current through S-CNT/PDMS-F and C-CNT/PDMS-F were highly linear over the tested voltage range which is in line with the classical Ohm's law. The greater gradient seen for S-CNT/PDMS-F curve further confirms its much lower electrical resistance as compared to C-CNT/PDMS-F.

### 3.3. Electromechanical performance of the strain sensors

The relative resistance change ($\Delta R/R_0$) was measured as a function of the applied strain. As shown in Fig. 5a, $\Delta R/R_0$ ratios of both sensors increased with increasing strain. Due to the combination of the highly stretchable elastic bandage and the elasticity of PDMS, both sensors could detect strains up to 200%. With S-CNT/PDMS-F having greater $\Delta R/R_0$

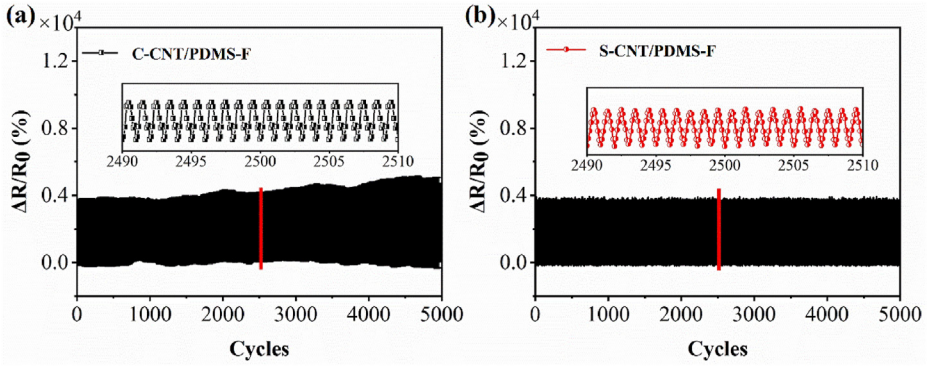


**Fig. 6.** Durability comparison between C-CNT/PDMS-F (a) and S-CNT/PDMS-F (b) after 5000 cycles at 50% strain under 1 Hz.

variation under the same applied strain. The GF of S-CNT/PDMS-F in the strain range of 0–100% reached 132, which is ~ 44% greater than that of C-CNT/PDMS-F (91.8). Within the strain range of 160–200%, the GF of S-CNT/PDMS-F reached 615, which is 2.42 times greater than that of C-CNT/PDMS-F ($GF_1 = 254$). The higher sensitivity of S-CNT/PDMS-F was likely due to presence of the self-segregated PDMS particles and the more rapid changes in the internal conductive network during the tensile stretching process. With increasing strain, the conductive pathways within the continuous CNT/PDMS phase would be narrowed/blocked [21] due to the reduced spacing between the self-segregated insulating PDMS particles. This would effectively impede electron transfer and lead to the greater resistance change and hence much higher sensitivity, comparing to the previous reports [25,31,32]. In addition, S-CNT/PDMS-F demonstrated a clear linear response within a reasonably wide strain range of 0–100% ($R^2 = 0.993$), suggesting the feasibility of easy linear calibration for such sensor.

Fig. 5b shows that S-CNT/PDMS-F had a more rapid response time (55 ms) as compared to C-CNT/PDMS-F (60 ms). The dynamic response behavior of the sensors was further characterized to evaluate their potential as a strain sensor in practical applications. The relationship

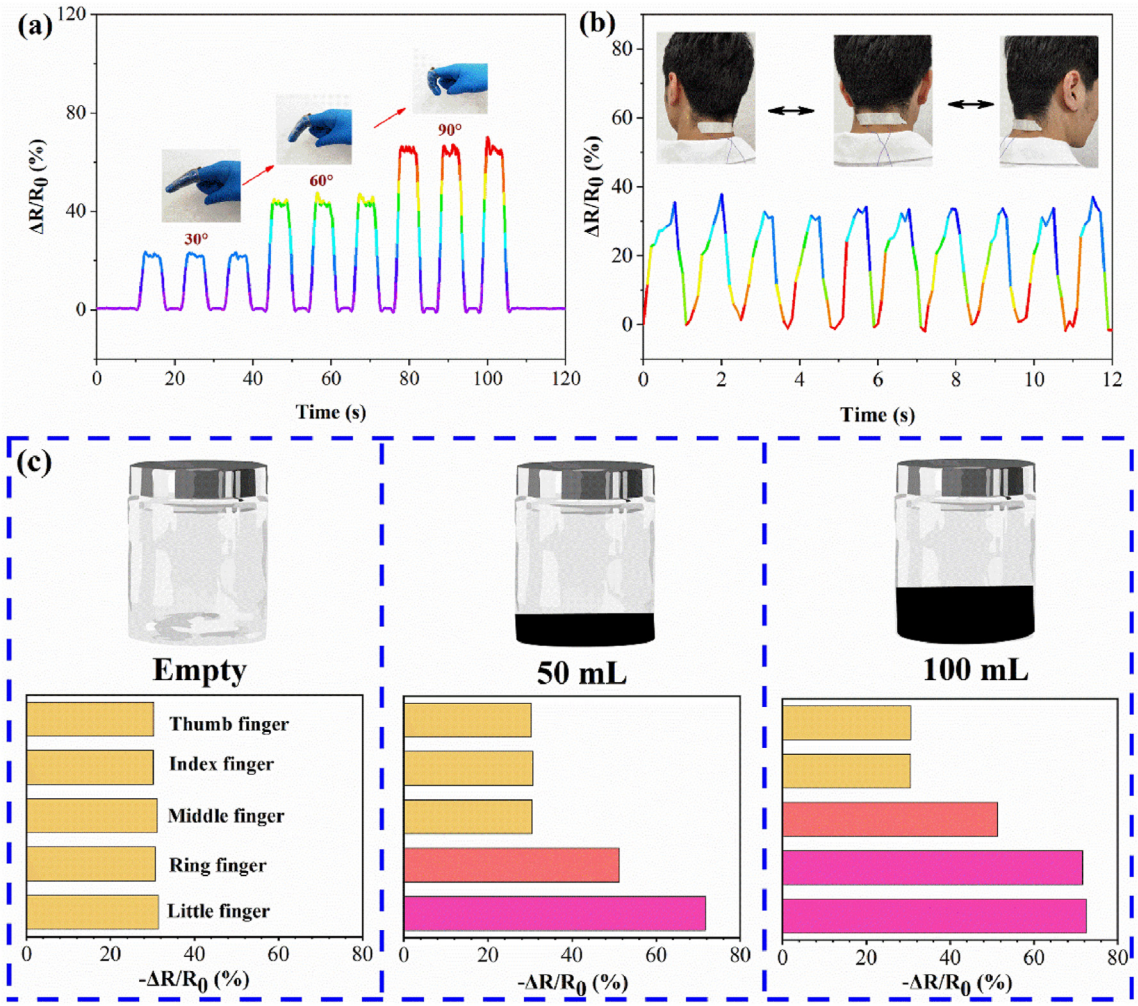


**Fig. 7.** $\Delta R/R_0$ of S-CNT/PDMS-F in different applications in monitoring (a) finger bending, (b) head movement and (c) finger pressures.

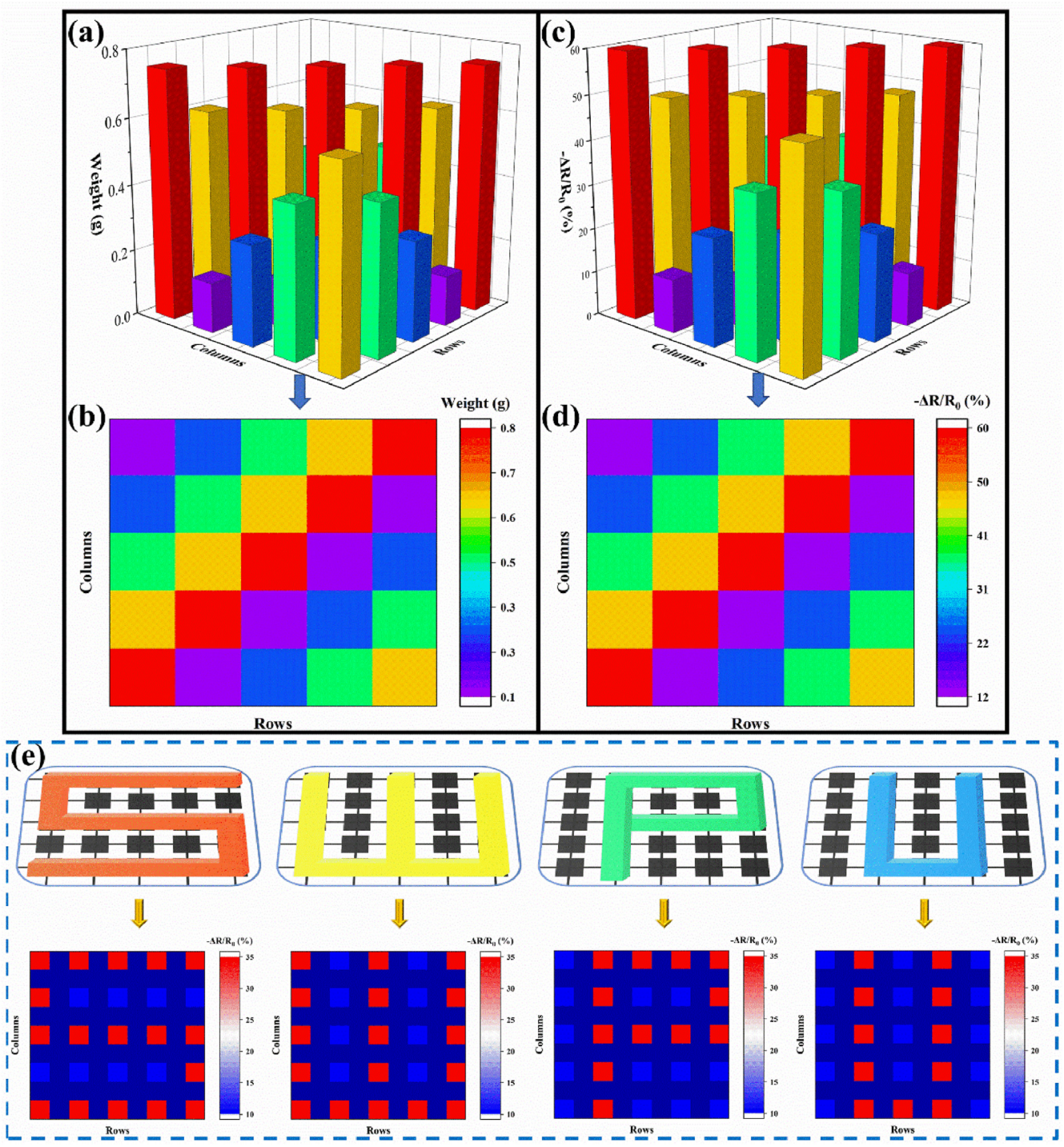


**Fig. 8.** Weight distribution sensing deploying S-CNT/PDMS-F. (a) and (b) Schematic diagram of objects with different weights, (c) and (d) corresponding electrical signal ($\Delta R/R_0$). (e) Electrical signal output for S-CNT/PDMS-F array sensors with different patterns.

between $\Delta R/R_0$ and frequency were analyzed at loading frequencies of 0.01, 0.1, 0.2 and 1Hz under 50% tensile strain, see Fig. 5c. Compared to C-CNT/PDMS-F, S-CNT/PDMS-F has a slightly higher relative resistance change and better stability. The high $\Delta R/R_0$ sensitivity of S-CNT/PDMS-F under different testing frequencies suggests it can be potentially used to monitor movements in different frequency domains.

The relationships between strain and $\Delta R/R_0$ of both sensors were investigated at a frequency of 0.1Hz, and the results are shown in Fig. 5d. The resistance response to different strains (5%, 10%, 30%, 50% and 80%) of both sensors showed a clear trend, i.e., the $\Delta R/R_0$ of the sensors increased with increasing applied strain. However, $\Delta R/R_0$ recorded for S-CNT/PDMS-F was higher than that of C-CNT/PDMS-F. The result indicates that S-CNT/PDMS-F is more sensitive than C-CNT/PDMS-F under the same strain testing conditions. The difference in sensitivity was again attributed to the self-segregated structure formed by the cross-linked PDMS phase in S-CNT/PDMS-F.

Dynamic cyclic loading tests were performed to estimate the repeatability and durability of both sensors and explore the effects of the self-segregated PDMS phase on the repeatability and durability of strain sensors. Fig. 6a and Fig. 6b show that $\Delta R/R_0$ of C-CNT/PDMS-F and S-CNT/PDMS-F, respectively, with a peak strain of 50% under a frequency of 1 Hz for 5000 loading/unloading cycles. Fig. 6a shows that after 1500

cycles, the resistance of C-CNT/PDMS-F increased significantly. This increase implies the deterioration of the conductive network structure within C-CNT/PDMS-F as the repeated deformation during the loading/unloading has led to irreversible damage to the sensor internal structure. In contrast, S-CNT/PDMS-F showed a more stable $\Delta R/R_0$ response throughout the test cycle (See Fig. 6b), demonstrating its excellent repeatability and durability. During loading/unloading cycles, the CNT network tended to be repeatedly disrupted/realigned in the in-plane direction along with the polymer chain movements. As a result, the conductive network was under repeated destruction and reconstruction. The presence of cross-linked PDMS self-segregated phase in S-CNT/PDMS-F compacted the CNTs within the conductive pathways, resulting in more concentrated and stable conductive network, which is more robust under the cyclic loading condition.

### 3.4. Applications

Given the more superior performance demonstrated by S-CNT/PDMS-F, it was selected for demonstration of practical applications. Fig. 7a displays the results of using S-CNT/PDMS-F for real time monitoring of finger bending. The sensor was attached to the index finger with different degrees of bending (30°, 60° and 90°). The corresponding electrical signal response increased with increasing degree of bending. Fig. 7b shows the application of S-CNT/PDMS-F for human head deflection monitoring (e.g. cervical spondylosis diagnosis). Individually addressable S-CNT/PDMS-F was also used for finger pressure test, see Fig. 7c. The sensors were attached to the fingers with adhesive tapes, and the pressure applied by each finger on the cup can be correlated to the $\Delta R/R_0$ of the sensor. With the addition of water, more pressure (and hence greater frictional force) is required to hold the cup. In addition, depending on the hand posture, the pressure imposed by each finger on different location of the cup was different, hence the $\Delta R/R_0$ of the sensor was also different [33]. Specifically, when the hand held an empty cup, the $\Delta R/R_0$ recorded for each finger was approximately the same, indicating that the evenly distributed pressure for all fingers. As the weight of the cup increases (volume of water increases in the cup), $\Delta R/R_0$ of the little finger showed the most significant increase, followed by the ring finger and the middle finger.

Going further, individually addressable S-CNT/PDMS-F could also be used to identify the weight distribution of different objects, as shown in Fig. 8. Fig. 8a and b show a schematic diagram of erasers with different weights placed on an array of S-CNT/PDMS-F sensors. Fig. 8c and d shows that the $\Delta R/R_0$ output signal at different position can be correlated to the weight of the object (greater weight resulting in greater $\Delta R/R_0$) and such feature could be deployed to produce sensor arrays with be-spoke patterns (see Fig. 8e).

## 4. Conclusion

By deploying self-segregated CNT/PDMS nanocomposite as a coating on highly elastic fabric based bandage, a new strategy is proposed for developing low cost, high performance S-CNT/PDMS-F strain sensor with ultrahigh sensitivity and wide strain detection range. The high sensitivity of the sensor (GF = 615) can be attributed to the presence of the self-segregated cross-linked PDMS particles within the nanocomposite coating. Apart from the large total strain detection range (up to 200%), the sensor also demonstrated a promising linear response within strain range 0–100% ($R^2 = 0.993$). In addition, compared with strain sensor without self-segregated PDMS, the developed S-CNT/PDMS-F has a faster response time, better signal output response under different frequencies and strains, and its signal stability, repeatability, and durability are improved. The excellent properties of the S-CNT/PDMS-F are also demonstrated for a wide ranging applications such as human movement monitoring, pressure monitoring and the load distribution recognition, etc.

## Declaration of competing interest

The authors declare that they have no known competing financial interests or personal relationships that could have appeared to influence the work reported in this paper.

## Acknowledgement

This work was supported by the National Natural Science Foundation of China (12102374), the National Key Research and Development Program (2019YFE0120300), the Sichuan Science and Technology Program (2021YFH0031), the International Cooperation Project of Chengdu (2019-GH02-00054-HZ), the Scientific Research Starting Project of SWPU (2019QHZ011) and Innovative Research Team of SWPU (2017CXTD01).

## References

[1] Z. Sun, S. Yang, P. Zhao, J. Zhang, Y. Yang, X. Ye, X. Zhao, N. Cui, Y. Tong, Y. Liu, X. Chen, Q. Tang, ACS Appl. Mater. Interfaces 12 (2020) 13287–13295, https://doi.org/10.1021/acsami.9b21751.
[2] D. Xiang, X. Zhang, E. Harkin-Jones, W. Zhu, Z. Zhou, Y. Shen, Y. Li, C. Zhao, P. Wang, Compos Part A Appl Sci Manuf 129 (2020), 105730, https://doi.org/10.1016/j.compositesa.2019.105730.
[3] Y. Cao, T. Lai, F. Teng, C. Liu, A. Li, Prog. Nat. Sci. 31 (2021) 379–386, https://doi.org/10.1016/j.pnsc.2021.05.005.
[4] Z. Sang, K. Ke, I. Manas-Zloczower, ACS Appl. Mater. Interfaces 10 (2018) 36483–36492, https://doi.org/10.1021/acsami.8b14573.
[5] T. Wang, Y. Zhang, Q. Liu, W. Cheng, X. Wang, L. Pan, B. Xu, H. Xu, A self-healable, Adv. Funct. Mater. 28 (2018), 1705551, https://doi.org/10.1002/adfm.201705551.
[6] Y. Wang, J. Hao, Z. Huang, G. Zheng, K. Dai, C. Liu, C. Shen, Carbon 126 (2018) 360–371, https://doi.org/10.1016/j.carbon.2017.10.034.
[7] X. Zhang, D. Xiang, W. Zhu, Y. Zheng, E. Harkin-Jones, P. Wang, C. Zhao, H. Li, B. Wang, Y. Li, Compos. Sci. Technol. 200 (2020), 108437, https://doi.org/10.1016/j.compscitech.2020.108437.
[8] Y. Fan, H. Zhao, F. Wei, Y. Yang, T. Ren, H. Tu, Prog. Nat. Sci. 30 (2020) 437–442, https://doi.org/10.1016/j.pnsc.2020.01.022.
[9] Y. Gao, F. Guo, P. Cao, J. Liu, D. Li, J. Wu, N. Wang, Y. Su, Y. Zhao, ACS Nano 14 (2020) 3442–3450, https://doi.org/10.1021/acsnano.9b09533.
[10] J. Gao, B. Li, X. Huang, L. Wang, L. Lin, H. Wang, H. Xue, Chem. Eng. J. 373 (2019) 298–306, https://doi.org/10.1016/j.cej.2019.05.045.
[11] Z. Sang, H. Guo, K. Ke, I. Manas-Zloczower, Macromol. Mater. Eng. 304 (2019), 1900278, https://doi.org/10.1002/mame.201900278.
[12] D. Xiang, X. Zhang, Y. Li, E. Harkin-Jones, Y. Zheng, L. Wang, C. Zhao, P. Wang, Compos. B Eng. 176 (2019), 107250, https://doi.org/10.1016/j.compositesb.2019.107250.
[13] S. Zhang, H. Liu, S. Yang, X. Shi, D. Zhang, C. Shan, L. Mi, C. Liu, C. Shen, Z. Guo, ACS Appl. Mater. Interfaces 11 (2019) 10922–10932, https://doi.org/10.1021/acsami.9b00900.
[14] I. Brook, R. Tchoudakov, R.Y. Suckeveriene, M. Narkis, Polym. Adv. Technol. 26 (2015) 889–897, https://doi.org/10.1002/pat.3526.
[15] Y. Zheng, Y. Li, Z. Li, Y. Wang, K. Dai, G. Zheng, C. Liu, C. Shen, Compos. Sci. Technol. 139 (2017) 64–73, https://doi.org/10.1016/j.compscitech.2016.12.014.
[16] G. Choi, H. Jang, S. Oh, H. Cho, H. Yoo, H.-I. Kang, Y. Choi, S.H. Kim, H.S. Lee, J. Mater. Chem. C. 7 (2019) 9504–9512, https://doi.org/10.1039/c9tc02486g.
[17] L. Wang, Y. Chen, L. Lin, H. Wang, X. Huang, H. Xue, J. Gao, Chem. Eng. J. 362 (2019) 89–98, https://doi.org/10.1016/j.cej.2019.01.014.
[18] J. Ma, P. Wang, H. Chen, S. Bao, W. Chen, H. Lu, ACS Appl. Mater. Interfaces 11 (2019) 8527–8536, https://doi.org/10.1021/acsami.8b20902.
[19] B. Mayoral, E. Harkin-Jones, P.N. Khanam, M.A. AlMaadeed, M. Ouederni, A.R. Hamilton, D. Sun, RSC Adv. 5 (2015) 52395–52409, https://doi.org/10.1039/c5ra08509h.
[20] M. He, X. Chen, Z. Guo, X. Qiu, Y. Yang, C. Su, N. Jiang, Y. Li, D. Sun, L. Zhang, Compos. Sci. Technol. 174 (2019) 194–201, https://doi.org/10.1016/j.compscitech.2019.02.028.
[21] M. Wang, K. Zhang, X.X. Dai, Y. Li, J. Guo, H. Liu, G.H. Li, Y.J. Tan, J.B. Zeng, Z. Guo, Nanoscale 9 (2017) 11017–11026, https://doi.org/10.1039/c7nr02322g.
[22] H. Zhang, D. Liu, J.-H. Lee, H. Chen, E. Kim, X. Shen, Q. Zheng, J. Yang, J.-K. Kim, Nano-Micro Lett. 13 (2021) 122, https://doi.org/10.1007/s40820-021-00615-5.
[23] Y. Zheng, Y. Li, K. Dai, Y. Wang, G. Zheng, C. Liu, C. Shen, Compos. Sci. Technol. 156 (2018) 276–286, https://doi.org/10.1016/j.compscitech.2018.01.019.
[24] D. Guo, X. Pan, H. He, Sens. Actuator A Phys. 298 (2019), 111608, https://doi.org/10.1016/j.sna.2019.111608.
[25] Y.-F. Chen, J. Li, Y.-J. Tan, J.-H. Cai, X.-H. Tang, J.-H. Liu, M. Wang, Compos. Sci. Technol. 177 (2019) 41–48, https://doi.org/10.1016/j.compscitech.2019.04.017.
[26] L. Zhang, Q. Zheng, X. Dong, X. Yu, Y. Wang, B. Han, Construct. Build. Mater. 256 (2020), 119452, https://doi.org/10.1016/j.conbuildmat.2020, 119452.
[27] X. Gao, S. Zhang, F. Mai, L. Lin, Y. Deng, H. Deng, Q. Fu, J. Mater. Chem. 21 (2011) 6401, https://doi.org/10.1039/c0jm04543h.

[28] S. Zhang, H. Deng, Q. Zhang, Q. Fu, ACS Appl. Mater. Interfaces 6 (2014) 6835–6844, https://doi.org/10.1021/am500651v.
[29] J. J. a. Jihun Hwang a, Kipyo Hong a, Kun Nyun Kim b, Jong Hun Han c, Kwonwoo Shin c, Chan Eon Park a, Carbon 49 (2011) 106–110, https://doi.org/10.1016/j.carbon.2010.08.048.
[30] H. Palza, C. Garzon, M. Rojas, Polym. Int. 65 (2016) 1441–1448, https://doi.org/10.1002/pi.5199.
[31] J. Chen, Y. Zhu, W. Jiang, Compos. Sci. Technol. 186 (2020), 107938, https://doi.org/10.1016/j.compscitech.2019.107938.
[32] Z. Ma, A. Wei, Y. Li, L. Shao, H. Zhang, X. Xiang, J. Wang, Q. Ren, S. Kang, D. Dong, J. Ma, G. Zhang, Compos. Sci. Technol. 203 (2021), 108571, https://doi.org/10.1016/j.compscitech.2020.108571.
[33] R. Wu, L. Ma, C. Hou, Z. Meng, W. Guo, W. Yu, R. Yu, F. Hu, X. Liu, Small 15 (2019), e1901558, https://doi.org/10.1002/smll.201901558.